Supplementary Materials

Optimizing multiscale resin flow kinetics and impregnation uniformity in fiber-reinforced polymers composites via hierarchical carbon nanostructures

Yu Zhang[1,#], Muhan Zhang[1,#], Helezi Zhou[1], Rongshan Zhou[1], Yiu Wing Mai[2], Huamin Zhou[1]

[1]State Key Laboratory of Material Processing and Die & Mold Technology, School of Materials Science and Engineering, Huazhong University of Science and Technology, Wuhan 430074, Hubei, China.
[2]Department of Mechanical Engineering & PolyU-SCUT Joint Research Center for Advanced and Green Composite Materials (CAGCOM), The Hong Kong Polytechnic University, Hong Kong 999077, China.
[#]These authors contributed equally to this work.

Correspondence to: Dr. Helezi Zhou, State Key Laboratory of Material Processing and Die & Mold Technology, School of Materials Science and Engineering, Huazhong University of Science and Technology, Wuhan 430074, Hubei, China. E-mail: helezizhou@hust.edu.cn; Dr. Yiu Wing Mai, Department of Mechanical Engineering & PolyU-SCUT Joint Research Center for Advanced and Green Composite Materials (CAGCOM), The Hong Kong Polytechnic University, Hong Kong 999077, China. E-mail: yw.mai@polyu.edu.hk

S1 Surface density of carbonaceous nanomaterials on fiber surfaces

To optimize the processing parameters, we examined the net weight change of CF fabrics treated *via* EPD and flame synthesis, and calculated the areal mass density of carbon nanomaterials deposited on the fiber preform, as shown in Figure S1. During the EPD process, GO particles are driven toward the fiber surface by the electrophoretic migration of charged ions. Increasing the electric-field strength can increase the electrophoretic drift velocity of the GO particles and accelerate their transport toward the surface. However, as the applied voltage or electrophoresis duration increases, the areal mass density initially rises and then declines [Figure S1A]. The optimal deposition conditions were determined to be a DC voltage of 15 V and an electrophoresis time of 15 min. The decrease at higher voltages is likely associated with bubble formation caused by water electrolysis, which interferes with particle adhesion on the fiber surface. Moreover, the rapid ion migration induced by elevated voltages may promote the aggregation of disordered particles, leading to the formation of a non-uniform deposition layer. Prolonged electrophoresis can also result in charge accumulation between deposited particles, causing electrostatic repulsion that inhibits further deposition. Excessive particle accumulation may concentrate local stresses within the coating, compromising its structural integrity. Additionally, prolonged electrolysis reduces the pH of the GO suspension, thereby destabilizing the colloidal system and significantly lowering deposition efficiency.

Figure S1B shows that the deposited CNT amount increases with higher concentrations of Ni^{+} catalyst and exhibits a nonmonotonic dependence on flame-treatment time. The yield initially increased but declined with prolonged exposure. In the initial stages of synthesis, carbon oxides adsorbed onto the catalyst surface were reduced to elemental carbon, which rapidly nucleated into CNT structures. Higher catalyst concentrations provided more active sites, thereby enhancing carbon conversion efficiency and promoting CNT growth. However, with extended combustion time, the nickel particles became progressively encapsulated by carbonaceous by-products, including CNTs and amorphous carbon, which gradually deactivated the catalytic sites and inhibited further CNT formation. Additionally, within the high-temperature flame core, some CNTs were subject to oxidation or thermal degradation,

reducing the overall yield. These dynamics resulted in a turning point in CNT mass density after approximately 90 s of combustion, identifying the optimal synthesis parameters as a nickel catalyst concentration of 0.4 mol·L^{-1} and a combustion duration of 90 s.

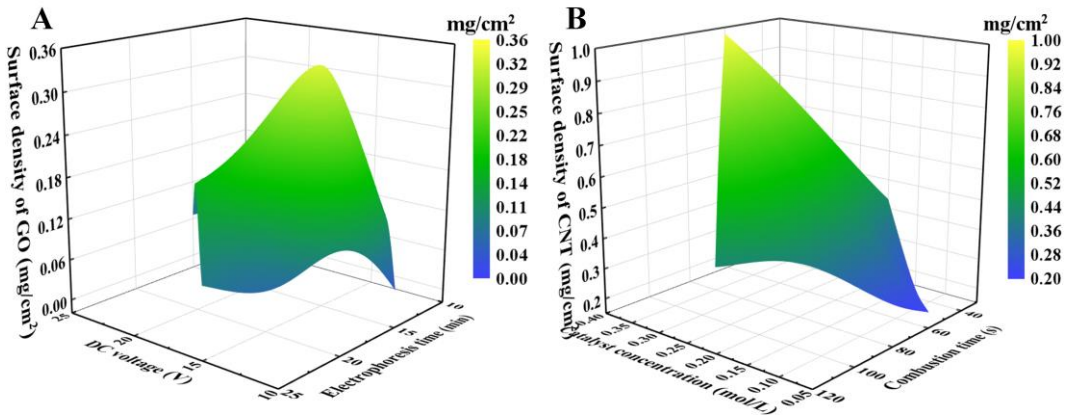

Figure S1. The net weight changes of woven fabric under different parameters (reflecting the mass density of carbon nanomaterials): (A) EPD method and (B) flame method.

S2 Capillary wicking of CF bundle

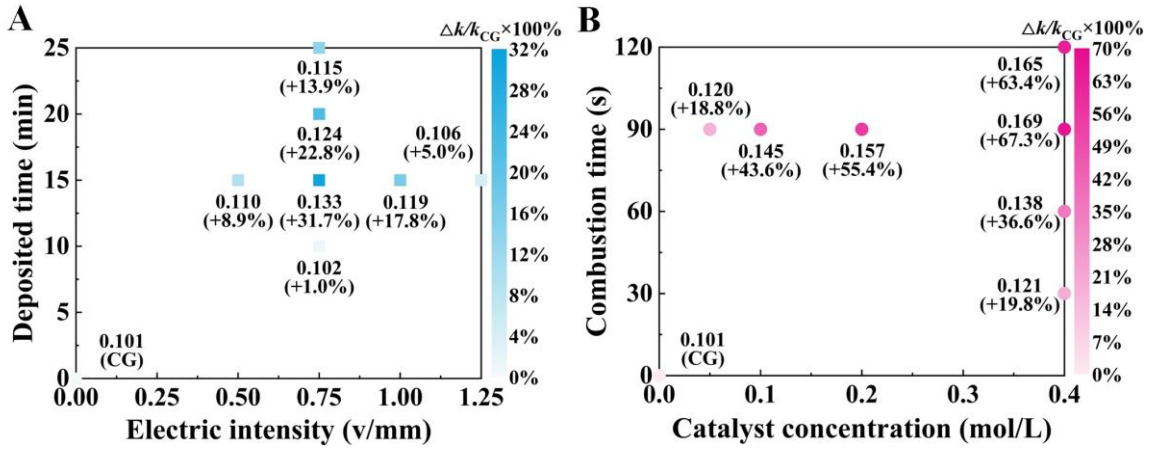

Figure S2. Variation of k_b with (A) EPD parameters, and (B) flame treatment parameters.

S3 Analysis of CFRP porosity

CFRP laminates were fabricated using VARI. Epoxy resin and curing agent were mixed at a mass ratio of 100:25 and infused into T300 fabrics under the pressure difference between the atmosphere and vacuum outlet. Twelve fabric plies were stacked in the same orientation, and the resulting laminates had a nominal thickness of 3.00-3.35 mm. The laminates were cured at 120 ℃ for 4 h. The laminate porosity ϕ was determined in accordance with ASTM D2734-

23 [1] from the difference between the calculated theoretical density and the measured laminate density:

$$\phi=\frac{100(\rho_{theoretical}-\rho_{measured})}{\rho_{theoretical}} \quad \text{(S1)}$$

where $\rho_{theoretical}$ and $\rho_{measured}$ are the theoretical and measured densities of the sample, respectively. $\rho_{theoretical}$ can be obtained from:

$$\rho_{theoretical}=\frac{100}{(\frac{\varphi_{resin}}{\rho_{resin}}+\frac{\varphi_{fiber}}{\rho_{fiber}})} \quad \text{(S2)}$$

where φ_{resin} and φ_{fiber} are the mass fractions of resin and fiber, respectively, while ρ_{resin} and ρ_{fiber} are the densities of resin and fiber, respectively. $\rho_{measured}$ can be indirectly evaluated from Archimedes water displacement principle [2]:

$$\rho_{measured}=\frac{W_a}{W_a-W_w} \quad \text{(S3)}$$

where W_a and W_w are the dry weight and saturated wet weight of the sample, respectively.

In the image-based porosity analysis of CFRP, porosity was quantified by estimating the geometric area ratio of pores identified in cross-sectional images, thereby providing an average representation of pore distribution within the material. The procedure involved capturing cross-sectional images of the CFRP specimen *via* OM, followed by importing the images into ImageJ software, where they were converted to 8-bit grayscale. The "Threshold" function was then applied for binary segmentation, isolating pore regions from the surrounding matrix, and the "Analyze Particles" tool was used to identify and measure the area of all detected pores. This enabled the calculation of the cumulative pore area, denoted as S_{voids}. Finally, ϕ was determined by normalizing the total pore area against the total cross-sectional area of the sample (S_{face}) using the following relation:

$$\phi=\frac{S_{voids}}{S_{face}}\times 100\% \quad \text{(S4)}$$

To ensure measurement consistency and reduce variability in the experimental results, four test samples, each measuring 10 mm×10 mm, were randomly selected from regions with

significant spatial dispersion across the surface of the laminates.

As illustrated in Figure S3A, the unmodified laminate exhibits distinct micro voids. By contrast, voids in the modified laminate are virtually eliminated. Figure S3B compares the porosity calculated by two methods. Both methods demonstrate that ϕ of $CFRP_{GO\text{-}CNT}$ was lower than that of $CFRP_{Received}$, with the porosity obtained by OM observation being slightly smaller than that derived from the density method. Notably, the OM results reveal only a slight reduction in porosity, indicating that GO-CNT modification has a limited capacity to eliminate micro voids. Nevertheless, the introduction of nanomaterials exerts no adverse effect on the formability of CFRP and helps balance the dual-scale flow, showing the potential to reduce porosity defects.

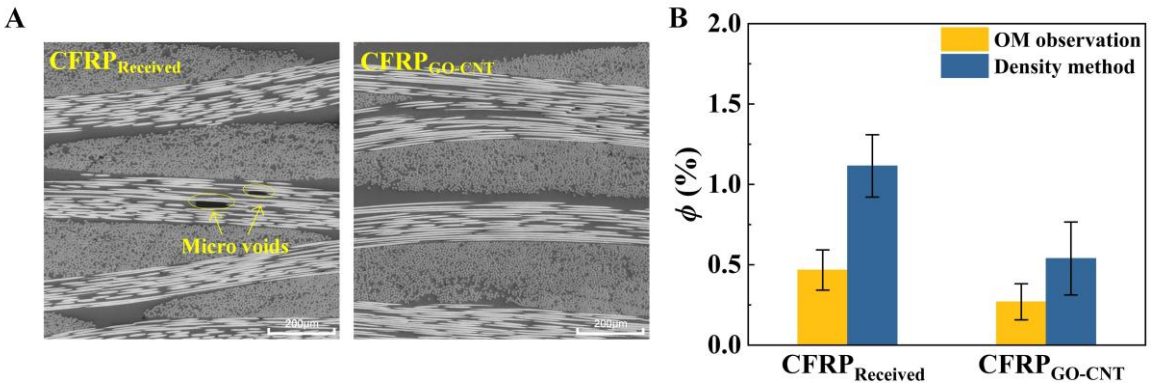

Figure S3. (A) Cross-sectional OM showing void distribution in $CFRP_{Received}$ and $CFRP_{GO\text{-}CNT}$; (B) comparison of porosity between $CFRP_{Received}$ and $CFRP_{GO\text{-}CNT}$ *via* OM observation density methods. The error bars represent the standard deviation (n=4).

REFERENCES

[1] ASTM D2734-23. Standard test methods for void content of reinforced plastics. West Conshohocken, PA: ASTM International, 2023.

[2] Saenz-Castillo, D.; Martín, M. I.; Calvo, S.; Rodriguez-Lence, F.; Güemes, A. Effect of processing parameters and void content on mechanical properties and NDI of thermoplastic composites. *Compos Part A Appl Sci Manuf* **2019**, *121*, 308–20. https://doi.org/10.1016/j.compositesa.2019.03.035.